Polymer Degradation and Stability 173 (2020) 109078

Contents lists available at ScienceDirect

Polymer Degradation and Stability

journal homepage: www.elsevier.com/locate/polydegstab

Sulfathiazole derivative with phosphaphenanthrene group: Synthesis, characterization and its high flame-retardant activity on epoxy resin

Peng Wang [a, b, *], Hang Xiao [a], Chao Duan [a], Bo Wen [a], Zongxin Li [a]

[a] College of Textile and Garment, Southwest University, Chongqing, 400715, PR China
[b] Chongqing Engineering Research Center of Biomaterial Fiber and Modern Textile, Chongqing, 400715, PR China

ARTICLE INFO

Article history:
Received 28 September 2019
Received in revised form
7 January 2020
Accepted 12 January 2020
Available online 13 January 2020

Keywords:
Epoxy resin
Sulfathiazole
Phosphaphenanthrene
Flame retardancy
Mechanism

ABSTRACT

A sulfathiazole derivative with phosphaphenanthrene group (STZ) was successfully synthesized by covalently bonding DOPO and imine intermediate obtained from the condensation of sulfathiazole with *p*-hydroxybenzaldehyde. Its effect on the thermal, flame-retardant and mechanical properties of epoxy thermosets were comprehensively studied. The presence of STZ decreased the initial degradation temperature and glass transition temperature (T_g) of epoxy thermoset. STZ significantly improved the flame retardancy and fire safety of epoxy thermoset. With the addition of only 4 wt% STZ, the modified epoxy thermoset achieved an LOI value of 29.1% and V-0 rating in UL-94 test. Moreover, the peak heat release rate (PHRR) and total heat release (THR) in cone calorimeter test were decreased by 34.4% and 32.1% in comparison with those of pure epoxy thermoset. STZ showed high flame-retardant activity not only by releasing nonflammable gases and phosphorous radicals in the gas phase, but also by promoting the formation of dense and intumescent char layer with honeycomb-like hollow structure inside in the condensed phase. Because of the strong intermolecular action between STZ and epoxy macromolecular chain, the presence of STZ increased the tensile strength, while decreased the elongation at break of epoxy thermoset.

© 2020 Elsevier Ltd. All rights reserved.

1. Introduction

Epoxy resins, as a prominent class of the most important thermosetting polymers, have found a variety of applications such as coatings, adhesives, electronics, electrical appliances and high performance composites because of their superior adhesion, chemical resistance, mechanical and dielectric properties [1,2]. Although epoxy resins possess so many excellent performance, their applications are still limited by high flammability and the release of a large amount of toxic gases and smoke during combustion [3]. To broaden their applications, it is imperative to improve the flame retardancy of epoxy resins by introducing flame retardants. Halogenated compounds were widely used to improve the flame retardancy of epoxy resins in the past. However, their use will result in a series of environment concerns as they produce poisonous and corrosive smoke during combustion [4,5]. To meet the requirement of environment-friendly principle, developing halogen-free flame retardants for epoxy resins has attracted increasing extensive attention [6].

Phosphorous compounds, due to their high efficiency, low production of corrosive and toxic gases during combustion, have been widely applied as environment-friendly halogen-free flame retardants for epoxy resins. They could exert flame-retardant effect either in the gas phase by scavenging active radicals to interrupt the combustion reaction, or in the condensed phase by altering the decomposition pathway of matrix and promoting the char formation [7]. As a prominent intermediate of phosphorous flame retardants, 9, 10-dihydro-9-oxa-10-phosphaphenanthrene-10-oxide (DOPO) has received a great deal of attention because of its high thermal stability, oxidation resistance, flame-retardant efficiency and multiple structural diversification by functionalization [8,9]. With active P—H bond in the structure, it could react with numerous electron-deficient compounds to construct DOPO derivatives with phosphorus- [6,10], nitrogen- [11,12], silicon- [13,14], and sulfur-containing groups [15], which have remarkably improved the flame retardancy of epoxy resins based on the synergism of flame-retardant groups.

Thiazole ring, as part of diverse five-membered heterocycles,

* Corresponding author. College of Textile and Garment, Southwest University, Chongqing, 400715, PR China.
E-mail address: wpeng3537@swu.edu.cn (P. Wang).

https://doi.org/10.1016/j.polymdegradstab.2020.109078
0141-3910/© 2020 Elsevier Ltd. All rights reserved.

has exerted a variety of roles in the lead identification and optimization, including as pharmacophoric group, bioisosteric element and spacer [16]. With nitrogen and sulfur elements, it shows an enormous potential in constructing highly efficient flame retardants. Recently, Ishida et al. reported a series of nonflammable functional benzoxazine resins with thiazole ring in their backbones. They all showed no ignition in UL-94 test and ultralow heat release capacity in microscale combustion calorimetry test [17]. Jian et al. reported a series of P/N/S-containing flame retardants with thiazole ring and phosphaphenanthrene or phosphamide group, which showed highly efficient flame-retardant activity both in the condensed and gas phases due to the synergism between thiazole ring and phosphorous group [18–20].

As one of the compounds containing thiazole ring, sulfathiazole possesses additional sulphone and amino groups, which make it possible to synthesize thiazole derivative with multiple flame-retardant elements by functionalization. Considering the synergism between phosphaphenanthrene and sulfur-containing group as demonstrated previously, it is reasonable to believe that the sulfathiazole derivative with phosphaphenanthrene group will show highly efficient flame-retardant activity for epoxy resin. Unfortunately, its synthesis, flame-retardant effect and mechanism on epoxy resin have rarely been reported in published literatures.

In this work, a sulfathiazole derivative with phosphaphenanthrene group (STZ) was synthesized by covalently bonding DOPO and imine intermediate obtained from the condensation of sulfathiazole with *p*-hydroxybenzaldehyde. With flame-retardant DOPO group and sulfathiazole moiety in the structure, STZ was employed to remarkably improve the flame retardancy and fire safety of epoxy resin. The effect of STZ on the thermal, flame-retardant and mechanical properties of epoxy thermosets were comprehensively studied. Moreover, the flame-retardant mechanism was particularly investigated by analyzing the pyrolysis and thermal-oxidative degradation products of STZ, the combustion behaviors of epoxy thermosets and the morphologies and structures of char residues.

2. Experimental

2.1. Materials

Tetraglycidyl diamino diphenyl methane epoxy resin (TGDDM, commercial name: JD919) with an epoxide equivalent weight of about 115 g/eq was purchased from Hunan Jiashengde Materials Technology Co., Ltd. DOPO was kindly provided by Jiangyin Hanfeng Technology Co., Ltd. Sulfathiazole, *p*-hydroxybenzaldehyde, 4,4′-diaminodiphenylsulfone (DDS) were all reagent grade, and obtained from Shanghai Aladdin Chemical Reagent Co., Ltd. Anhydrous ethanol was supplied by Chengdu Kelong Chemicals Co., Ltd.

2.2. Synthesis of STZ

STZ was synthesized via a one-pot method, and its synthesis pathway was shown in Scheme 1. Briefly, sulfathiazole (25 mmol, 6.38 g) dissolved in anhydrous ethanol (300 mL) was introduced into a 500 mL three-neck round-bottomed glass flask equipped with a magnetic stirrer and a reflux condenser. With the temperature increasing to 85 °C, *p*-hydroxybenzaldehyde (25 mmol, 3.05 g) was added into the flask and stirred for 6 h to obtain the imine intermediate (not isolated). Subsequently, DOPO (25 mmol, 5.40 g) was charged into the above reaction mixture and stirred for another 18 h. Successively, the reaction system was slowly cooled down to room temperature. The precipitate was filtered, washed with ethanol and dried at 70 °C for 24 h in a vacuum oven (yield: 94%).

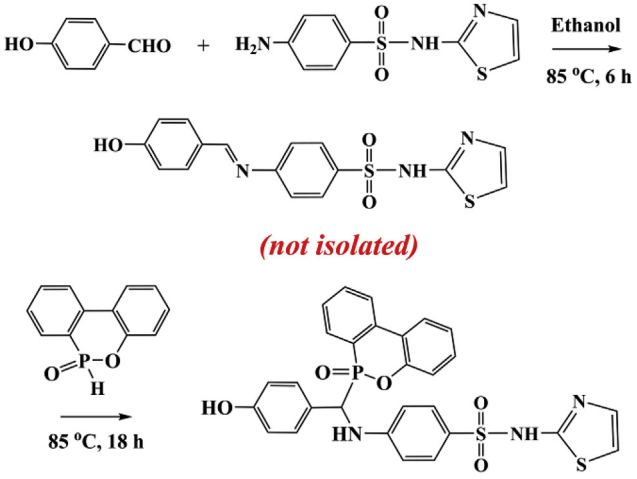

Scheme 1. The synthesis pathway of STZ.

2.3. Preparation of epoxy thermosets

Formulations of epoxy thermosets are listed in Table 1. The flame-retardant epoxy thermoset with *x* wt% STZ was designated as EP/STZ*x*, and it was prepared via traditional thermal curing process. Specifically, TGDDM and STZ were introduced into a 250 mL three-neck round-bottomed glass flask equipped with a mechanical stirrer and stirred at 160 °C until STZ was dissolved in epoxy resin completely. With the temperature raising to 185 °C, DDS was charged into the mixture and stirred for 2 min to form homogeneous liquid. After the mixture was degassed in a vacuum oven, it was poured into preheated stainless steel moulds and cured at 150 °C for 3 h and 180 °C for 3 h. The control sample (EP) and thermoset modified with DOPO were also prepared using similar process.

2.4. Characterization

The FTIR spectra were obtained using a Bruker ALPHA spectrometer (Bruker, Switzerland) at frequencies ranging from 4000 to 400 cm^{-1}. Samples were mixed with KBr and pressed into pellets.

The ^{1}H, ^{13}C and ^{31}P NMR spectra were recorded on a Bruker AVANCE III 600 spectrometer (Bruker, Switzerland) using DMSO-d_6 as solvent and tetramethylsilane (TMS) as internal standard.

Elemental analyses (C, H, N and S) were determined on an Elementar Vario EL Cube elemental analyzer (Elementar Analysensysteme GmbH, Germany). The content of phosphorus was measured on an Agilent 730 inductively coupled plasma-atomic emission spectrometer (Agilent, USA).

Thermogravimetric analysis (TGA) of sample about 10.0 mg was performed on a TG 209 F3 thermal analyzer (Netzsch, Germany) from 30 °C to 600 °C at a heating rate of 10 °C/min under constant nitrogen flow of 60 mL/min. TG-FTIR analysis was conducted on a Nicolet iS10 FTIR spectrometer (Thermo Fischer, USA), connected

Table 1
Formulations of epoxy thermosets.

Sample	Composition (g)				STZ (wt%)	DOPO (wt%)
	TGDDM	DDS	STZ	DOPO		
EP	100	53.98	0	0	0	0
EP/STZ2	100	53.98	3.14	0	2	0
EP/STZ4	100	53.98	6.42	0	4	0
EP/STZ6	100	53.98	9.83	0	6	0
EP/DOPO4	100	53.98	0	6.42	0	4

with a TG 209 F3 thermal analyzer through a heated transfer line maintained at 250 °C.

Differential scanning calorimetry analysis (DSC) of sample about 5.0 mg was performed with a DSC Q25 instrument (TA, USA) at a heating rate of 10 °C/min from 20 °C to 300 °C under nitrogen atmosphere.

LOI test was carried out on an M606B digital oxygen index instrument (Qingdao Shanfang Instrument Co., Ltd., China) according to ASTM D2863-06, with a specimen bar of 130 × 6.5 × 3 mm^3. The UL-94 vertical burning test was performed according to GB/T 2408-2008, with a specimen bar of 130 × 12.7 × 3 mm^3. Cone calorimeter test was conducted on an FTT0007 cone calorimetry (FTT, UK) according to ISO 5660. The sample mounted on an aluminium foil with dimension of 100 × 100 × 3 mm^3 was exposed to a radiant cone at an incident radiant flux of 35 kW/m^2, and the relevant data were averaged from three measurements.

Py-GC/MS analysis was carried out on a Frontier Lab EGA/PY-3030D pyrolyser coupled to a Shimadzu GC-MS QP-2010 Ultra. The sample about 2.0 mg was pyrolyzed at 600 °C for 20 s in the pyrolysis furnace before the volatiles were introduced into the GC/MS. High purity helium (99.999%) was used as the carrier gas at a constant flow rate of 1 mL/min. For the separation, the heating program of capillary column (DB-5MS) was as follows: 40 °C for 3 min, and then heated to 280 °C with a heating rate of 15 °C/min and held for 10 min.

Microstructure of char residue after UL-94 test was observed using a Hitachi S-4800 scanning electron microscope (Hitachi, Japan) under high vacuum condition with a voltage of 20 kV.

X-ray photoelectron spectroscopy (XPS) spectrum was measured by an ESCALAB 250Xi spectrometer (Thermo Fischer, USA) with a monochromatic AlKα source ($h\nu$ = 1253.6 eV).

The tensile test was conducted on a E44.104 electromechanical universal testing machine (MTS, China) at a constant speed of 5 mm/min according to ASTM D638-08, and the relevant data were averaged from five measurements.

3. Results and discussion

3.1. Characterization of STZ

The chemical structure of STZ was characterized by FTIR, ^{1}H NMR, ^{13}C NMR, ^{31}P NMR and elemental analysis. Fig. 1a shows the FTIR spectrum of STZ. The typical absorption peaks of DOPO group appear at 1596, 1477 (P–C_{Ar}), 1199, 930 (P–O–C_{Ar}), 1285 (P=O) and 751 cm^{-1} (C_{Ar}–H deformation of ortho-substituted aromatic ring). The peak at 3345 cm^{-1} is assigned to the stretching vibration of O–H bond. The peaks at 1330 and 1145 cm^{-1} correspond to the stretching vibration of O=S=O bond [21]. Fig. 1b depicts the ^{1}H

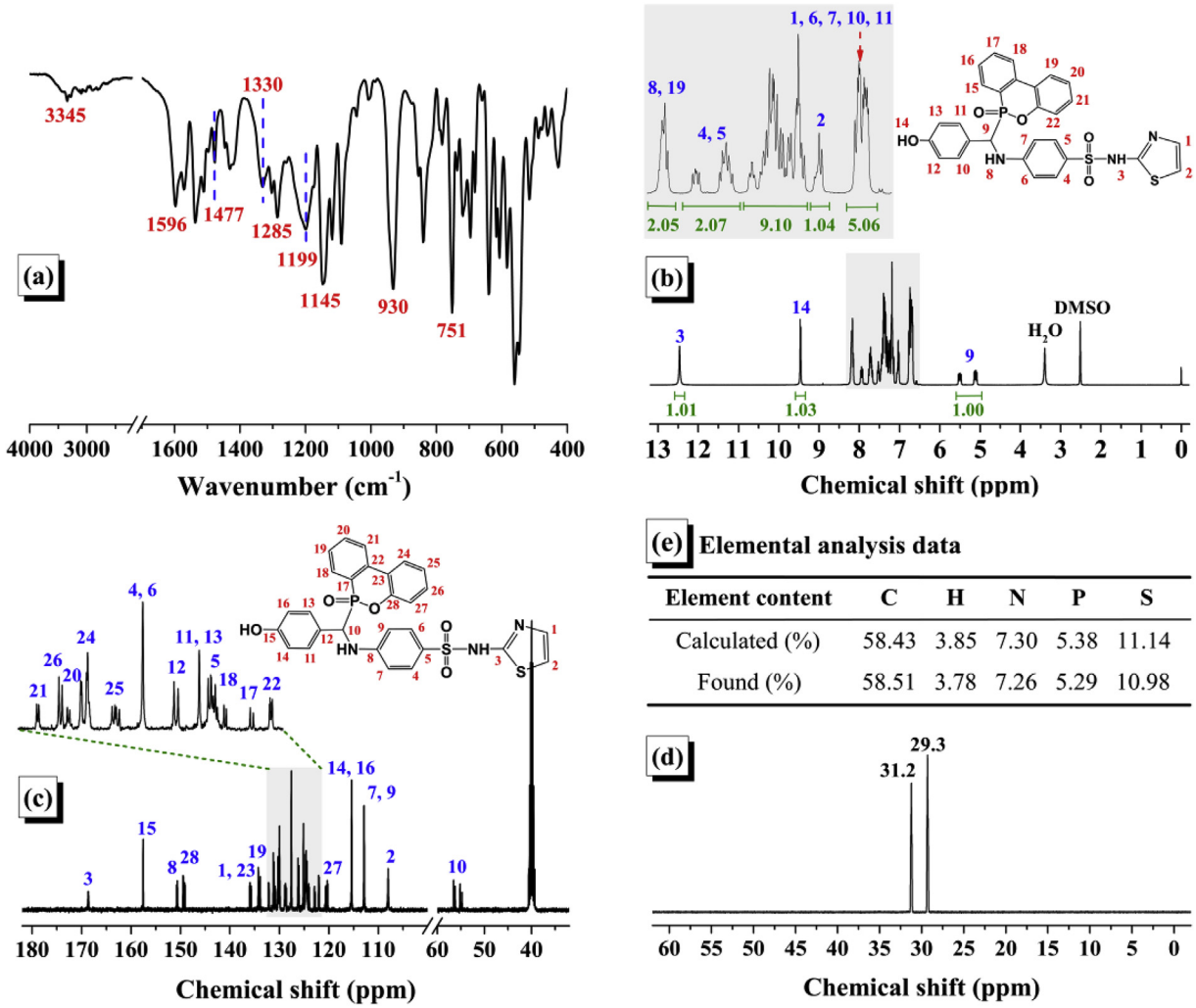

(e) Elemental analysis data

Element content	C	H	N	P	S
Calculated (%)	58.43	3.85	7.30	5.38	11.14
Found (%)	58.51	3.78	7.26	5.29	10.98

Fig. 1. FTIR (a), ^{1}H NMR (b), ^{13}C NMR (c), ^{31}P NMR (d) spectra and elemental analysis data (e) of STZ.

NMR spectrum of STZ and the possible assignment of protons. The multiple peaks at 5.05–5.58 ppm correspond to the proton (H9) in methine group linked with phosphorus atom. The proton (H14) in phenolic hydroxyl group appears at 9.46 ppm. The peak at 12.46 ppm is due to the proton (H3) linked with O═S═O group. The ratio of integrated areas is 1.00: 1.03:1.01 for H9, H14 and H3, which coincides with the number ratio of corresponding protons. The other protons in the structure are also well assigned in the spectrum, as shown in Fig. 1b. In the ^{13}C NMR spectrum as shown in Fig. 1c, the peak at 168.6 ppm is assigned to the quaternary carbon (C3) in thiazole ring. The peaks due to tertiary carbon atoms (C1, C2) in thiazole ring appear at 136.0 and 108.0 ppm, respectively. The multiple peaks in 54.6–56.6 ppm are due to the tertiary carbon atom (C10) in methine group linked with phosphorus atom. The other peaks belong to the carbon atoms in aromatic rings. Two peaks at 29.3 and 31.2 ppm assigned to the phosphorus atom in DOPO group are observed in the ^{31}P NMR spectrum as shown in Fig. 1d. This suggests the formation of diastereomers with unequal phosphorus peaks, which possibly results from the existence of chiral carbon atom [22,23]. The elemental contents were further analyzed to confirm the chemical structure of STZ. It reveals that the found values coincide well with the calculated values as shown in Fig. 1e. These data above all give the evidence that STZ has been synthesized successfully.

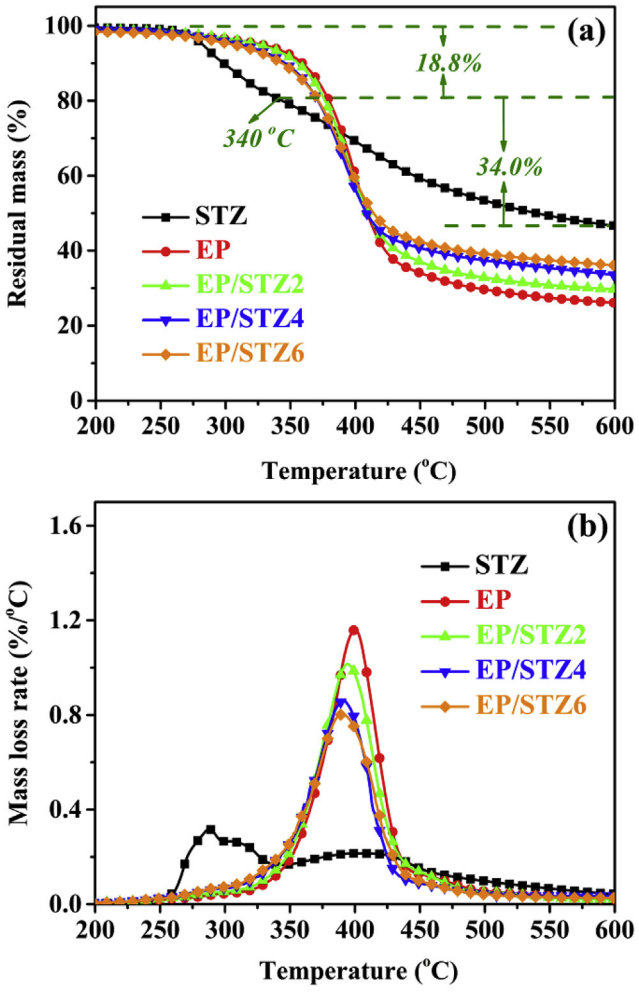

Fig. 2. TG (a) and DTG (b) curves of STZ and epoxy thermosets in nitrogen.

3.2. Thermal properties

The thermal stabilities of STZ and epoxy thermosets under nitrogen atmosphere were assessed by thermogravimetric analysis. Fig. 2 plots the TG and DTG curves of STZ and epoxy thermosets, and the relevant data are given in Table 2. It can be observed that STZ starts to degrade at around 260 °C with a $T_{5\%}$ (the temperature of 5% mass loss) of 285.5 °C. Its degradation process can be divided into two stages according to DTG curve. The first stage happens in the region of 260–340 °C, which is due to the decomposition of sulfathiazole moiety. The second stage appears in the region of 340–600 °C, and the mass loss is 34.0%. Apart from the further decomposition of sulfathiazole moiety, the second stage also includes the decomposition of DOPO group, which will be disclosed in the following section.

Pure EP undergoes a one-step degradation process with a T_{max} (the temperature at the maximum mass loss rate) of 400.2 °C, which corresponds to the thermal degradation of macromolecular chains through dehydration and chain scission reactions [24,25]. Modified thermoset shows a similar degradation process to pure EP. However, it is noteworthy that the presence of STZ results in the early degradation of epoxy thermoset, and the $T_{5\%}$ value of modified thermoset decreases with the increase of STZ content. As previously reported, the O═P–O bond in DOPO derivative is less stable than the common C–C bond in epoxy matrix [26]. Moreover, the steric hindrance of bulky DOPO pendant and thiazole ring results in the decrease of crosslinking density of thermoset [27,28]. These two factors are responsible for the reduction of $T_{5\%}$ value for modified thermoset. Compared to pure EP, modified thermoset achieves a lower V_{max} (the maximum mass loss rate) and a higher CY_{600} (the char yield at 600 °C), suggesting that the presence of STZ inhibits the degradation of epoxy matrix and contributes to the char formation [29]. It is possible that the early degradation of STZ releases phosphorus-containing acid, which reacts with epoxy matrix to promote the formation of char layer [30]. The char layer isolates underlying matrix from heat to postpone the degradation of matrix.

The glass transition behaviors of epoxy thermosets were investigated by DSC. The glass transition temperature (T_g) is taken as the midpoint in the specific heat capacity transition, and the corresponding data are given in Table 2. Pure EP obtains a T_g of 255.3 °C, and the value is in line with the reported cured TGDDM/DDS system [31]. The presence of STZ lowers the T_g of epoxy thermoset, and it decreases from 253.7 °C for EP/STZ2 to 250.9 °C for EP/STZ6. As mentioned previously, STZ possesses a high steric hindrance because of the existence of bulky DOPO pendant and thiazole ring in the structure, which may restrain the curing reaction between TGDDM and DDS, thus resulting in the decrease of crosslinking density of epoxy network. This phenomenon was also reported in epoxy thermoset modified with DOPO derivative [27,32]. The decrease in crosslinking density accounts for the decrease of T_g.

3.3. Flame-retardant properties

The flame-retardant properties of pure EP and modified epoxy

Table 2
Thermal data of STZ and epoxy thermosets in nitrogen.

Sample	$T_{5\%}$ (°C)	T_{max} (°C)	V_{max} (%/°C)	CY_{600} (%)	T_g (°C)
STZ	285.5	288.3, 400.2	0.32, 0.22	47.2	–
EP	327.9	400.2	1.16	26.5	255.3
EP/STZ2	320.6	394.1	1.01	29.4	253.7
EP/STZ4	308.7	391.7	0.86	33.3	252.1
EP/STZ6	305.2	390.2	0.80	36.1	250.9

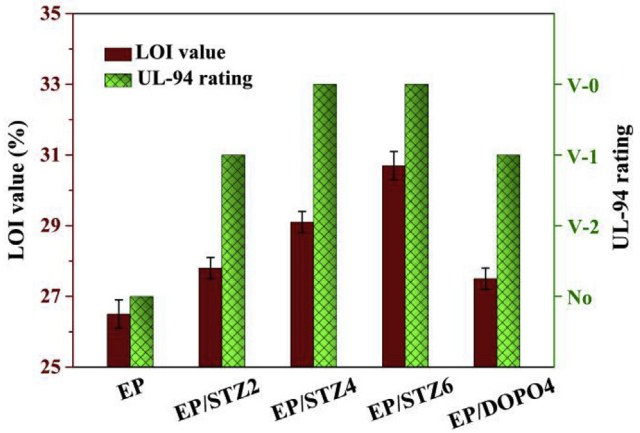

Fig. 3. LOI values and UL-94 ratings of pure EP and modified epoxy thermosets.

thermosets were comprehensively evaluated through LOI, UL-94 and cone calorimetry tests.

Fig. 3 and Table 3 show the LOI and UL-94 data of pure EP and modified thermosets. Pure EP achieves an LOI value of 26.5% and no rating in UL-94 test. It burns vigorously after ignition, and flaming drips are observed during UL-94 test. For modified thermoset, the LOI value increases with the increase of STZ content. It increases from 27.8% for EP/STZ2 to 29.1% for EP/STZ4, and further increases to 30.7% for EP/STZ6. The incorporation of STZ results in the disappearance of flaming drips during UL-94 test for epoxy thermoset. With the incorporation of only 4 wt% STZ, the corresponding thermoset passes V-0 rating in UL-94 test. Moreover, EP/DOPO4 achieves a lower LOI value and UL-94 rating than EP/STZ4. These data demonstrate that STZ possesses high flame-retardant activity, and efficiently improves the flame retardancy of epoxy thermoset. Fig. 4 presents the video screenshots of pure EP and EP/STZ4 during UL-94 test. It can be found that pure EP burns vigorously with flaming drips. EP/STZ4 generates massive gases around burning matrix within a few seconds after ignition. Then, the flame is seemingly blown out by the ejected gases from the surface of burning matrix. Similar blowing out phenomena have also been observed in other epoxy thermosets modified with DOPO derivatives during combustion [13,33]. It is deduced that the blowing out phenomenon closely accounts for the superior flame retardancy of modified thermoset, which will be disclosed in the following part.

As the most significant bench scale way to assess the fire performance of materials, cone calorimeter test provides detailed information related to the fire hazard, such as time to ignition (TTI), heat release rate (HRR), peak HRR (PHRR), time to peak PHRR (t-PHRR), total heat release (THR), fire growth rate (FGR=PHRR/t-PHRR), average effective heat of combustion (av-EHC), average CO yield (av-COY) and average CO_2 yield (av-CO_2Y).

Fig. 5 plots the HRR and THR versus time curves of epoxy thermosets, and the corresponding data are summarized in Table 4. Modified thermoset achieves a shorter TTI than pure EP, which possibly results from the early degradation of modified thermoset induced by STZ as mentioned in TGA [34]. Pure EP obtains a PHRR of 893.2 kW/m^2 and a THR of 57.0 MJ/m^2. The PHRR and THR of EP/STZ4 are decreased by 34.4% and 32.1% in comparison with those of pure EP. Besides, the FGR and TSP of modified thermoset are lower than those of pure EP, which suggests that the presence of STZ suppresses the fire spreading and smoke formation during combustion, thus improving the fire safety of epoxy thermoset. The smoke suppression mechanism of STZ may be attributed to its

Table 3
LOI and UL-94 data of epoxy thermosets.

Sample	LOI (%)	UL-94, 3.0 mm bar		
		[a] t_1+t_2 (s)	Dripping	Rating
EP	26.5 ± 0.4	>100	Yes	No
EP/STZ2	27.8 ± 0.3	12.9	No	V-1
EP/STZ4	29.1 ± 0.3	8.8	No	V-0
EP/STZ6	30.7 ± 0.4	5.4	No	V-0
EP/DOPO4	27.5 ± 0.3	20.7	No	V-1

[a] t_1+t_2, average total combustion time after two applications of the flame.

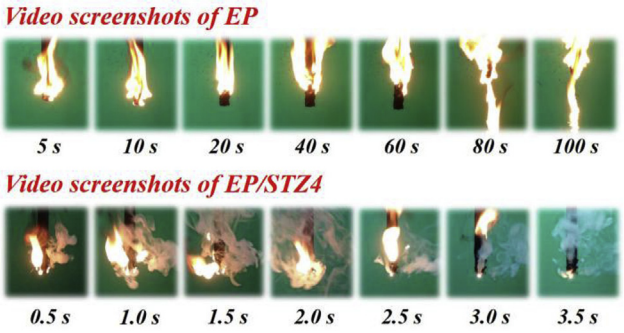

Fig. 4. Video screenshots of pure EP and EP/STZ4 during UL-94 test.

catalytic charring effect, which blocks the diffusion of pyrolysis products and isolates the unburned matrix beneath from fire during combustion [35]. The av-EHC reflects the combustion degree of volatiles in the gas phase, which is useful for analysis of gaseous flame-retardant mechanism. It is noteworthy that the presence of STZ results in the reduction of av-EHC, which suggests that STZ shows flame-retardant activity in the gas phase. Moreover, modified thermoset achieves a higher av-COY, while a lower av-CO_2Y than pure EP. This means that the presence of STZ results in incomplete combustion of volatiles during combustion, which further confirms the gaseous flame-retardant effect of STZ. For epoxy thermosets, the residual mass increases with the increase of STZ content. For instance, it increases from 27.7% for pure EP to 36.7% for EP/STZ6, demonstrating that STZ also exerts flame-retardant effect in the condensed phase by promoting the formation of char layer. In conclusion, the incorporation of STZ improves the flame retardancy and fire safety of epoxy thermoset. STZ shows flame-retardant activity both in the gas and condensed phases.

3.4. Flame-retardant mechanism analysis

3.4.1. Gaseous pyrolysis products of STZ

TG-FTIR analysis provides useful information about the volatiles during pyrolysis. To disclose the flame-retardant role in the gas phase as suggested above, TG-FTIR was used to analyze the gaseous products of STZ during pyrolysis.

Fig. 6 shows the data obtained from TG-FTIR analysis of STZ, including three dimensional diagram and FTIR spectra of volatiles at different temperatures. It is clear that some absorption peaks are detected in the spectrum at 280 °C, since STZ starts to degrade at around 260 °C as mentioned in TGA. It can be found that CO_2 (2400-2200 cm^{-1}), COS (2100-2000 cm^{-1}), NO_2 (1617 cm^{-1}) [36], CS_2 (1560-1460 cm^{-1}), SO_2 (1400-1300 cm^{-1}) [37], NH_3 (965, 931 cm^{-1}) are detected in the temperature range of 280–310 °C. Similar gaseous products were also observed during the pyrolysis of compounds with thiazole ring [38]. These gaseous products may originate from the pyrolysis of sulfathiazole moiety. With the

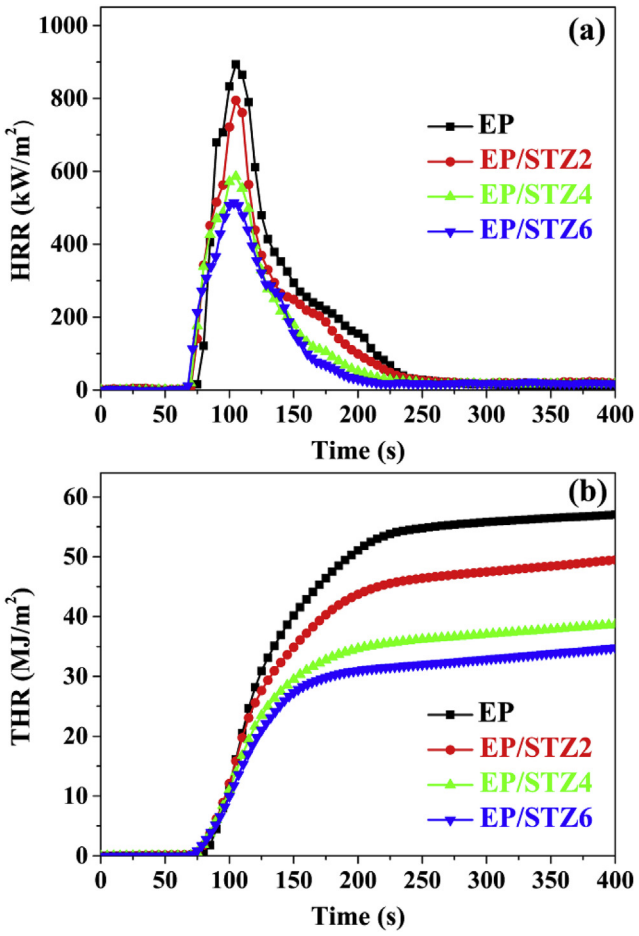

Fig. 5. HRR (a) and THR (b) versus time curves of epoxy thermosets.

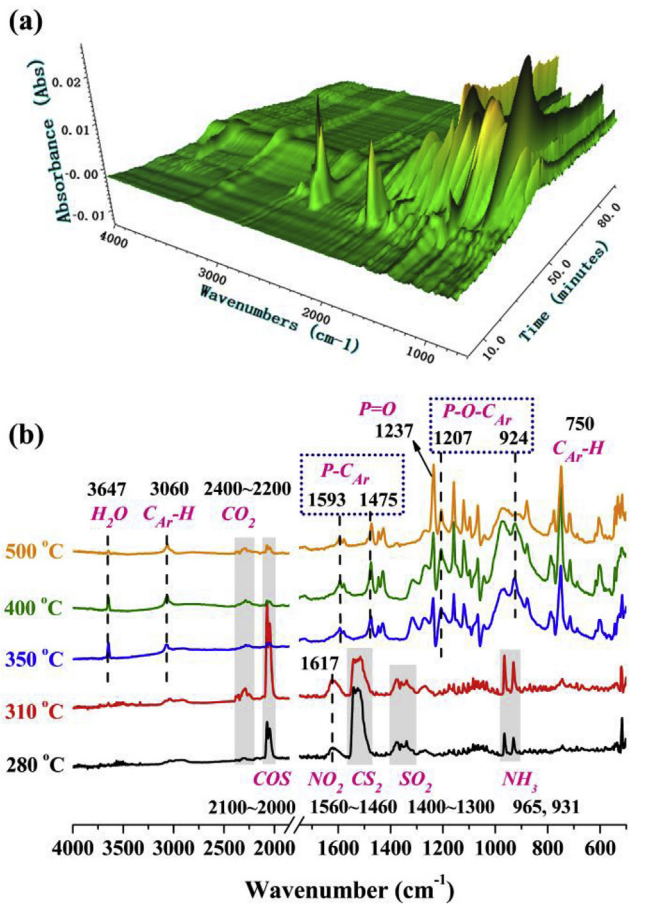

Fig. 6. Three dimensional diagram (a) and FTIR spectra (b) of volatiles at different temperatures of STZ during pyrolysis.

Table 4
Cone calorimetry data of epoxy thermosets.

Sample	EP	EP/STZ2	EP/STZ4	EP/STZ6
TTI (s)	65 ± 4	62 ± 3	56 ± 5	51 ± 3
PHRR (kW/m^2)	893.2 ± 51.3	794.4 ± 43.2	585.5 ± 27.5	513.8 ± 33.8
t-PHRR (s)	105 ± 3	105 ± 5	105 ± 5	103 ± 5
THR (MJ/m^2)	57.0 ± 3.2	49.5 ± 1.5	38.7 ± 2.6	34.8 ± 1.8
FGR (kW/(m^2·s))	8.5 ± 0.7	7.6 ± 0.7	5.6 ± 0.5	5.3 ± 0.3
av-EHC (MJ/kg)	19.5 ± 0.5	18.1 ± 0.8	16.2 ± 0.4	15.5 ± 0.6
av-COY (kg/kg)	0.08 ± 0.02	0.11 ± 0.01	0.12 ± 0.02	0.14 ± 0.02
av-CO_2Y (kg/kg)	1.62 ± 0.07	1.48 ± 0.04	1.46 ± 0.02	1.41 ± 0.05
Residual mass (%)	27.7 ± 2.2	32.4 ± 0.8	35.1 ± 0.4	36.7 ± 1.7
TSP (m^2)	18.5 ± 0.6	16.6 ± 1.0	14.4 ± 0.7	13.3 ± 1.2

temperature increasing to 350 °C, apart from the peaks due to the absorptions of CO_2 and COS, some new peaks are found at 3647, 3060, 1593, 1475, 1237, 1207, 924 and 750 cm^{-1}. Moreover, the relative intensities of these peaks first increase and then decrease with the increase of temperature. The maximum intensity appears at about 400 °C, indicating that the decomposition of STZ is the most intensive near this temperature, which is in accordance with TGA data. The peak at 3647 cm^{-1} confirms the existence of H_2O in the volatiles. The peaks at 1593, 1475 (P–C_{Ar}), 1207, 924 (P–O–C_{Ar}), 1237 (P=O) and 3060, 750 cm^{-1} (C_{Ar}–H vibration from the ortho-substituted aromatic ring) are assigned to the typical absorptions of DOPO group. These data above demonstrate that STZ releases nonflammable gases (CO_2, H_2O, NO_2, SO_2, NH_3) and DOPO derivatives in the gas phase during pyrolysis.

Py-GC/MS test was carried out to further characterize the gaseous pyrolysis products of STZ. Fig. 7a shows the pyrogram and assigned pyrolysis products of STZ. It clearly reveals that the detected pyrolysis products are SO_2, COS, CS_2, biphenyl, *o*-phenylphenol, dibenzofuran, fluorene, nitrogenous compounds (4, 6) and DOPO derivatives (13, 15, 16). In contrast to the gaseous products detected in TG-FTIR analysis, the inexistence of NH_3 may be ascribed to its low molecular weight, which is beyond the detection limit of Py-GC/MS analysis. In consideration of the chemical structure of STZ, it is believable that SO_2, COS and CS_2 originate from the pyrolysis of sulfathiazole moiety. Biphenyl, *o*-phenylphenol, dibenzofuran and fluorene come from the pyrolysis of DOPO moiety. DOPO derivatives (13, 15, 16) may stem from the scission of chemical bonds or the rearrangement of free radicals generated during pyrolysis. For instance, the rupture of P–C and P–O bonds in DOPO moiety results in the formation of dibenzofuran [39], and the scission of C–C and C–N bonds in STZ accounts for the formation of 6-methyldibenzo[c,e] [1,2]oxaphosphinine 6-oxide (13). As reported previously, the rupture of P–C bond in DOPO derivative leads to the elimination of DOPO free radical in the gas phase, which proceeds to generate biphenylene and dibenzofuran by the removal of PO_2 and PO radicals [33,40], as shown in Fig. 7b. The appearance of dibenzofuran in the pyrolysis products further gives the evidence that phosphorous radicals really exist in the gas phase during pyrolysis of STZ [41,42].

Based on the above TG-FTIR and Py-GC/MS analyses, it is reasonable to conclude that the sulfur element and nitrogen element in STZ transform into sulfur-containing gases like SO_2 and

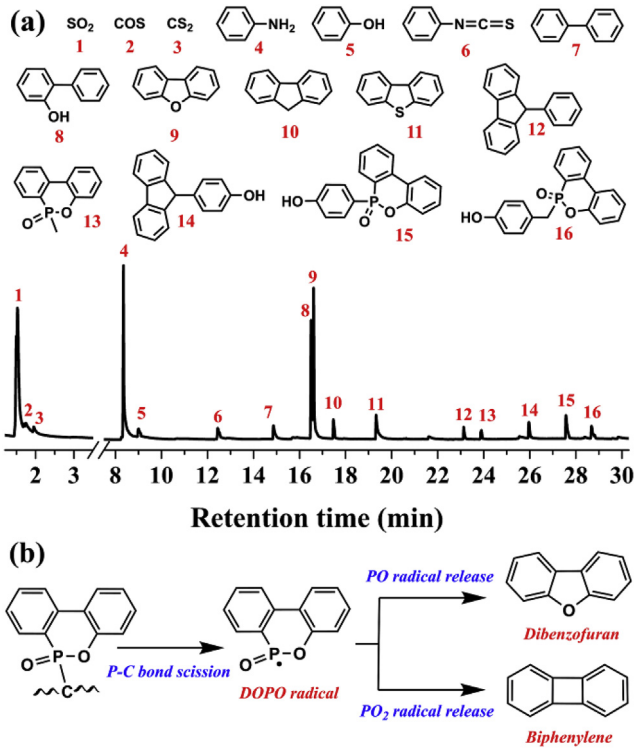

Fig. 7. (a) The pyrogram and assigned pyrolysis products of STZ, (b) possible formation route of phosphorous radicals.

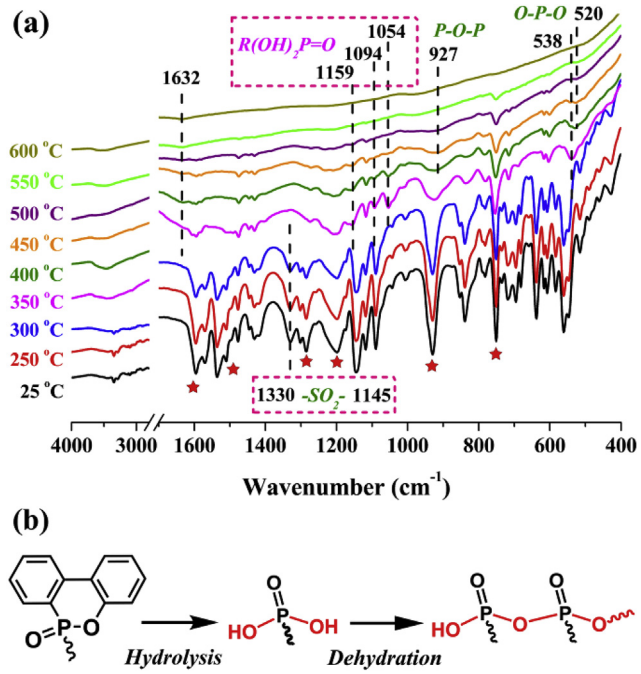

Fig. 8. (a) FTIR spectra of STZ at different temperatures in air, (b) possible formation route of phosphorous compounds with P—OH bond.

nitrogen-containing gases like NH_3 during pyrolysis, respectively. STZ exerts gaseous flame-retardant effect by producing nonflammable gases (CO_2, H_2O, NO_2, SO_2, NH_3) and phosphorous radicals (PO and PO_2 radicals). The nonflammable gases cut off the supply of oxygen, dilute the fuels and take away the heat. The phosphorous radicals not only scavenge active radicals (H and OH radicals) to interrupt the combustion reaction, but also combine with active terminal radicals in the decomposed molecular chain of matrix to suppress its further decomposition [43–45].

3.4.2. Condensed thermo-oxidative degradation products of STZ

Investigation of the thermo-oxidative degradation behavior of STZ provides information about the chemical composition of char residues generated at different temperatures in air, which will contribute to understanding its flame-retardant effect in the condensed phase. To illustrate the thermo-oxidative degradation behavior of STZ, the char residues obtained at different temperatures in air were analyzed. STZ was heated at a rate of 10 °C/min from room temperature to 600 °C in air. The char residues were collected when heated to a specified temperature and characterized via FTIR.

Fig. 8 displays the FTIR spectra of STZ at different temperatures in air and possible formation route of phosphorous compounds with P—OH bond. At 250 °C, the spectrum appears nearly the same as that at room temperature, which suggests that STZ is stable near this temperature. At 350 °C, the peaks at 1330 and 1145 cm^{-1} assigned to the stretching vibration of O=S=O bond vanish, implying the release of SO_2 due to the breakage of sulfonyl group in the gas phase below this temperature [46]. In contrast to the spectrum at room temperature, the relative intensities of typical absorption peaks (marked with red five-pointed star) of DOPO group decrease obviously at 350 °C, suggesting that DOPO moiety is partly released to the gas phase due to the rupture of P—C bond, which has been suggested in TG-FTIR analysis. Moreover, some new peaks (1632, 1159, 1094, 1054, 538 cm^{-1}) are detected in the spectrum, which correspond to the typical absorptions of P—OH bond. The peaks at 1159, 1094 and 1054 cm^{-1} are indicative of the existence of phosphoric acid derivatives with $R(OH)_2P{=}O$ group [47], which possibly result from the hydrolysis of DOPO moiety [48]. With the temperature raising to 400 °C, the spectrum appears two additional peaks at 927 and 520 cm^{-1} in comparison with the spectrum at 350 °C, which are due to the absorptions of P—O—P bond and O—P—O bond [49], respectively. This confirms the formation of polyphosphoric acid derivatives due to the dehydration of P—OH bond.

These data above demonstrate that STZ generates phosphoric acid derivatives with reactive P—OH bond during the thermo-oxidative degradation, which proceed to form polyphosphoric acid derivatives through the dehydration of P—OH bond. These phosphorous compounds with reactive P—OH bond react with epoxy matrix to promote the char formation, thus playing flame-retardant role in the condensed phase.

3.4.3. Morphology and structure of char residue

Analyses of morphology and structure of char residue could contribute to further disclosing the flame-retardant mechanism. Fig. 9 shows the digital and SEM images of char residues of pure EP and EP/STZ4 obtained after UL-94 and cone calorimeter tests. As shown in Fig. 9a, the char residue of EP/STZ4 shows an intumescent morphology, and the amount of char residue is higher than that of pure EP, which has been confirmed by cone calorimetry data in Table 4. For the char residues obtained after UL-94 test as shown in Fig. 9b, pure EP burns completely and shows little char residue with a discontinuous structure both in the exterior and interior. EP/STZ4 nearly retains its previous morphology, and some broken bulgy stomas appear on the surface of char residue. In view of the video screenshots of EP/STZ4 during UL-94 test in Fig. 4, it is believable that high-speed ejected airflows from burning matrix result in the broken bulgy stomas on the surface. The external char residue of

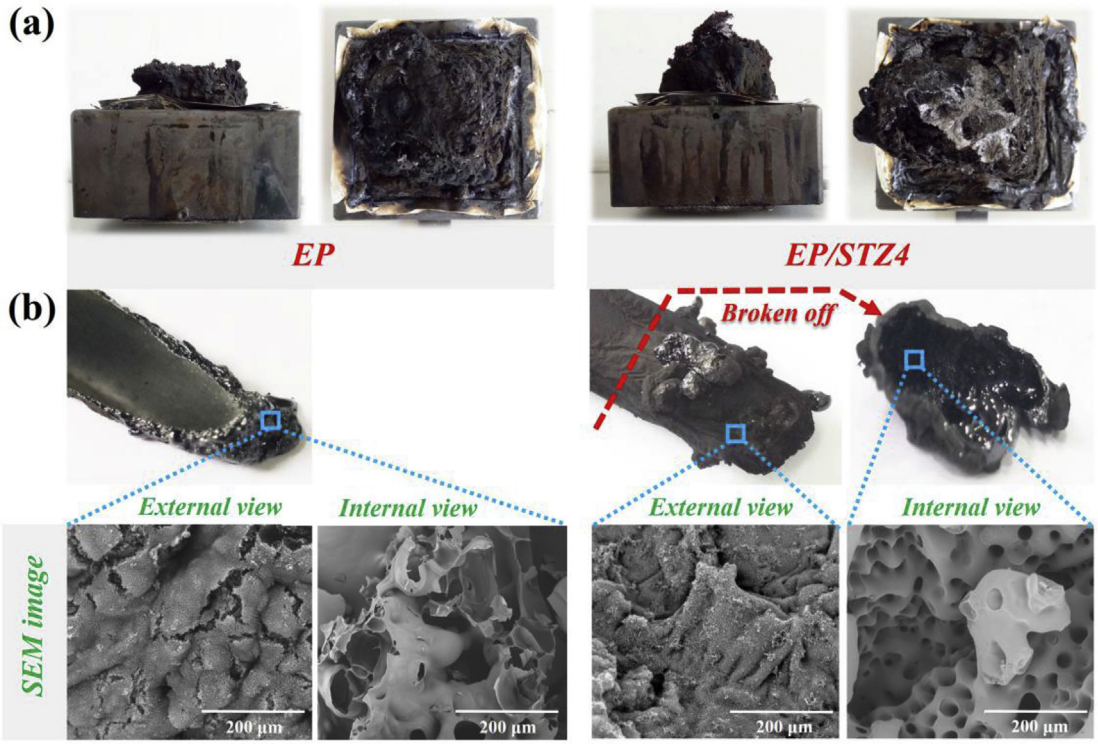

Fig. 9. Images of char residues generated after cone calorimeter (a) and UL-94 (b) tests.

EP/STZ4 is compact and dense as shown in SEM image. To observe the morphology of char residue in the interior of EP/STZ4, a tweezer was employed to break off the sample bar. It is of surprise to note that the char residue displays hollow structure in the interior. Moreover, the micromorphology presented in SEM image reveals that the internal char residue shows honeycombed structure with massive holes running through. This dense char layer with honeycomb-like hollow structure inside plays a pivotal role in improving the flame retardancy of epoxy thermoset. On the one hand, it acts as a thermally insulating layer to isolate the matrix from heat and fuels. On the other hand, it stores huge amounts of gases with massive phosphorous radicals and nonflammable gases during combustion, which are intensively released to blow out the flame when the gas pressure in the interior is high enough to break through the char layer.

XPS analysis was used to investigate the chemical composition of char residue. Fig. 10 shows the XPS spectra of char residues of pure EP and EP/STZ4 after cone calorimeter test. The char residue of pure EP consists of carbon, oxygen, nitrogen and sulfur elements. It should be noted that apart from carbon, oxygen, nitrogen and sulfur elements, phosphorus element is detected in the char residue of EP/STZ4. To disclose the chemical environment of sulfur and phosphorus atoms, the S2p and P2p XPS spectra were fitted using Gaussian-Lorentzian function. S2p XPS spectrum shows two peaks at 164.4 and 168.7 eV, which are assigned to thiophene group and sulfonyl group, respectively [50,51]. Two peaks at 134.2 and 133.5 eV are observed in the P2p XPS spectrum. The peak at 134.2 eV corresponds to P—O—P bond [19], which generates from the dehydration of P—OH bond as mentioned above. The peak at 133.5 eV is assigned to P—O—C bond [52], which gives the evidence that phosphorous compounds with reactive P—OH bond generated during the thermo-oxidative degradation of STZ really react with epoxy matrix by esterification and dehydration to promote the char formation.

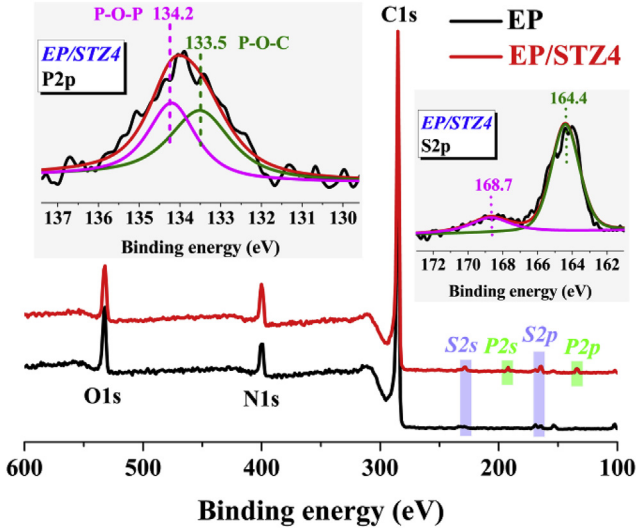

Fig. 10. XPS spectra of char residues generated after cone calorimeter test.

3.5. Flame-retardant mechanism

Fig. 11 shows the schematic illustration of flame-retardant mechanism. STZ exerts gaseous flame-retardant effect by releasing nonflammable gases like SO_2 and NH_3, and phosphorous radicals like PO and PO_2 radicals. The nonflammable gases cut off the supply of oxygen, dilute the fuels and take away the heat. The phosphorous radicals capture H and OH radicals in the flame zone, and interrupt the free radical chain reaction of combustion. Moreover, it also shows flame-retardant activity by generating phosphorous compounds with reactive P—OH bond in the condensed phase, which react with decomposed epoxy matrix to

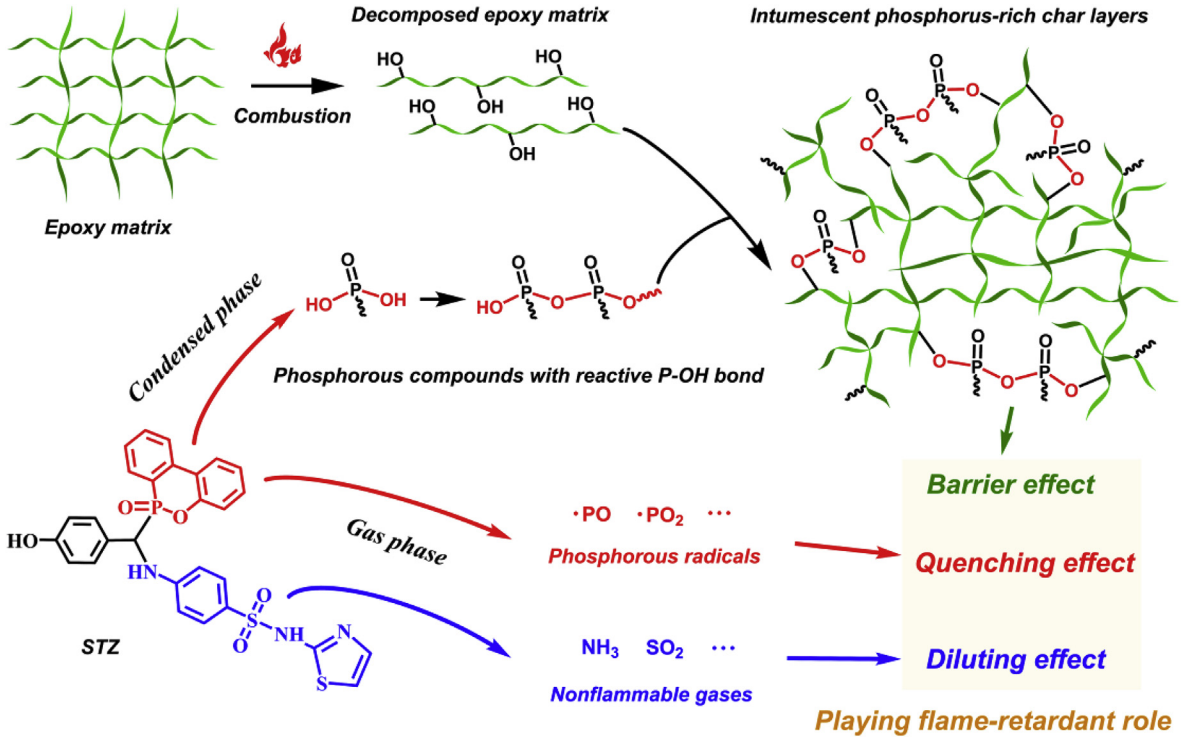

Fig. 11. Schematic illustration of flame-retardant mechanism.

promote the formation of dense and intumescent char layer. This char layer with honeycomb-like cavity inside not only acts as a superior physical barrier to isolate the matrix from heat and fuels, but also stores huge amounts of gases containing considerable phosphorous radicals and nonflammable gases during combustion. The gases inside are released intensively to blow out the flame when the inner gas pressure is high enough to break through the char layer, accompanied by the appearance of blowing out phenomenon. Thus, the remarkable flame retardancy of epoxy thermoset modified with STZ benefits from the barrier effect of intumescent phosphorus-rich char layers, quenching effect of phosphorous radicals and diluting effect of nonflammable gases.

3.6. Mechanical properties

The tensile test was conducted to disclose the effect of STZ on the mechanical property of epoxy thermoset. Fig. 12 and Table 5 present the relevant data of epoxy thermosets, including the tensile strength and elongation at break. The presence of STZ leads to the increase of tensile strength, while the decrease of elongation at break. For instance, the tensile strength increases from 52.8 MPa for pure EP to 60.9 MPa for EP/STZ6, while the elongation at break decreases from 3.3% to 2.4%. As mentioned above, the steric hindrance of bulky DOPO pendant and thiazole ring in STZ results in the decrease of crosslinking density of epoxy thermoset, which is bad for the improvement of tensile strength. However, STZ owns multiple aromatic rings and heteroatoms (N, S and O) in the structure, which form additional π-π interaction and hydrogen bonding with epoxy matrix [15,53]. The formation of strong intermolecular action between STZ and epoxy macromolecular chain is beneficial for the improvement of tensile strength. These two competing factors eventually result in the increase of tensile strength of modified epoxy thermoset.

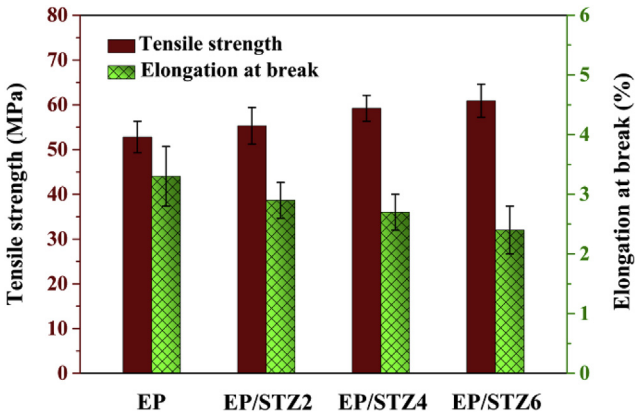

Fig. 12. Tensile data of pure EP and modified epoxy thermosets.

Table 5
Tensile strength and elongation at break data of epoxy thermosets.

Sample	EP	EP/STZ2	EP/STZ4	EP/STZ6
Tensile strength (MPa)	52.8 ± 3.5	55.3 ± 4.1	59.2 ± 2.9	60.9 ± 3.7
Elongation at break (%)	3.3 ± 0.5	2.9 ± 0.3	2.7 ± 0.3	2.4 ± 0.4

4. Conclusions

In summary, a sulfathiazole derivative with phosphaphenanthrene group was synthesized, and used to remarkably improve the flame retardancy and fire safety of epoxy resin. The presence of STZ decreased the initial degradation temperature and T_g of epoxy thermoset. With the incorporation of only 4 wt% STZ, the modified epoxy thermoset obtained an LOI value of 29.1% and passed UL-94 V-0 rating. The PHRR and THR were decreased by 34.4% and 32.1%

in contrast to those of pure EP. With DOPO group and sulfathiazole moiety in the structure, STZ showed high flame-retardant activity both in the gas and condensed phases. It played flame-retardant role not only by releasing nonflammable gases (SO_2, NH_3) and phosphorous radicals (PO and PO_2 radicals), but also by promoting the formation of dense and intumescent char layer with honeycomb-like hollow structure inside. Modified thermoset showed interesting blowing out phenomenon during combustion. It was the intensive release of gases that blew out the flame based on the diluting effect of nonflammable gases and quenching effect of phosphorous radicals. Moreover, the presence of STZ resulted in the increase of tensile strength, while the decrease of elongation at break of epoxy thermoset.

Declaration of interests

The authors declare that they have no known competing financial interests or personal relationships that could have appeared to influence the work reported in this paper.

CRediT authorship contribution statement

Peng Wang: Conceptualization, Methodology, Software, Writing - original draft, Supervision. **Hang Xiao:** Validation, Formal analysis, Writing - review & editing, Visualization. **Chao Duan:** Investigation, Formal analysis, Visualization. **Bo Wen:** Investigation, Resources, Data curation. **Zongxin Li:** Investigation, Data curation.

Acknowledgments

This work was financially supported by the National Natural Science Foundation of China (Grant No. 21905233) and the Fundamental Research Funds for the Central Universities (Grant Nos. XDJK2020C024, SWU117028 and SWU118070).

References

[1] S. Wang, S.Q. Ma, C.X. Xu, Y. Liu, J.Y. Dai, Z.B. Wang, et al., Vanillin-derived high-performance flame retardant epoxy resins: facile synthesis and properties, Macromolecules 50 (5) (2017) 1892–1901.
[2] S. Liu, V.S. Chevali, Z. Xu, D. Hui, H. Wang, A review of extending performance of epoxy resins using carbon nanomaterials, Compos. B Eng. 136 (2018) 197–214.
[3] K.Q. Zhou, G. Tang, R. Gao, S.D. Jiang, In situ growth of 0D silica nanospheres on 2D molybdenum disulfide nanosheets: towards reducing fire hazards of epoxy resin, J. Hazard Mater. 344 (2018) 1078–1089.
[4] J. Artner, M. Ciesielski, O. Walter, M. Döring, R.M. Perez, J.K.W. Sandler, et al., A novel DOPO-based diamine as hardener and flame retardant for epoxy resin systems, Macromol. Mater. Eng. 293 (6) (2008) 503–514.
[5] Y.-O. Kim, J.Y. Cho, H. Yeo, B.W. Lee, B.J. Moon, Y.M. Ha, et al., Flame retardant epoxy derived from tannic acid as biobased hardener, ACS Sustain. Chem. Eng. 7 (4) (2019) 3858–3865.
[6] Y. Zhang, B. Yu, B.B. Wang, K.M. Liew, L. Song, C.M. Wang, et al., Highly effective P-P synergy of a novel DOPO-based flame retardant for epoxy resin, Ind. Eng. Chem. Res. 56 (5) (2017) 1245–1255.
[7] C. Ma, S.L. Qiu, B. Yu, J.L. Wang, C.M. Wang, W.R. Zeng, et al., Economical and environment-friendly synthesis of a novel hyperbranched poly(-aminomethylphosphine oxide-amine) as co-curing agent for simultaneous improvement of fire safety, glass transition temperature and toughness of epoxy resins, Chem. Eng. J. 322 (2017) 618–631.
[8] X. Wang, Y. Hu, L. Song, W.Y. Xing, H.D. Lu, P. Lv, et al., Flame retardancy and thermal degradation mechanism of epoxy resin composites based on a DOPO substituted organophosphorus oligomer, Polymer 51 (11) (2010) 2435–2445.
[9] P. Wang, Z.S. Cai, Highly efficient flame-retardant epoxy resin with a novel DOPO-based triazole compound: thermal stability, flame retardancy and mechanism, Polym. Degrad. Stab. 137 (2017) 138–150.
[10] J.L. Wang, C. Ma, P.L. Wang, S.L. Qiu, W. Cai, Y. Hu, Ultra-low phosphorus loading to achieve the superior flame retardancy of epoxy resin, Polym. Degrad. Stab. 149 (2018) 119–128.
[11] P. Wang, L. Chen, H. Xiao, Flame retardant effect and mechanism of a novel DOPO based tetrazole derivative on epoxy resin, J. Anal. Appl. Pyrolysis 139 (2019) 104–113.
[12] Y.Q. Xiong, Z.J. Jiang, Y.Y. Xie, X.Y. Zhang, W.J. Xu, Development of a DOPO-containing melamine epoxy hardeners and its thermal and flame-retardant properties of cured products, J. Appl. Polym. Sci. 127 (6) (2013) 4352–4358.
[13] W.C. Zhang, X.M. Li, R.J. Yang, Novel flame retardancy effects of DOPO-POSS on epoxy resins, Polym. Degrad. Stab. 96 (12) (2011) 2167–2173.
[14] P.J. Chao, Y.J. Li, X.Y. Gu, D.D. Han, X.Q. Jia, M.Q. Wang, et al., Novel phosphorus–nitrogen–silicon flame retardants and their application in cycloaliphatic epoxy systems, Polym. Chem. 6 (15) (2015) 2977–2985.
[15] R.K. Jian, Y.F. Ai, L. Xia, Z.P. Zhang, D.Y. Wang, Organophosphorus heteroaromatic compound towards mechanically reinforced and low-flammability epoxy resin, Compos. B Eng. 168 (2019) 458–466.
[16] A. Ayati, S. Emami, A. Asadipour, A. Shafiee, A. Foroumadi, Recent applications of 1,3-thiazole core structure in the identification of new lead compounds and drug discovery, Eur. J. Med. Chem. 97 (2015) 699–718.
[17] F. Shan, S.S. Ohashi, A. Erlichman, H. Ishida, Non-flammable thiazole-functional monobenzoxazines: synthesis, polymerization, thermal and thermomechanical properties, and flammability studies, Polymer 157 (2018) 38–49.
[18] R.K. Jian, P. Wang, L. Xia, X.L. Zheng, Effect of a novel P/N/S-containing reactive flame retardant on curing behavior, thermal and flame-retardant properties of epoxy resin, J. Anal. Appl. Pyrolysis 127 (2017) 360–368.
[19] P. Wang, L. Xia, R.K. Jian, Y.F. Ai, X.L. Zheng, G.L. Chen, et al., Flame-retarding epoxy resin with an efficient P/N/S-containing flame retardant: preparation, thermal stability, and flame retardance, Polym. Degrad. Stab. 149 (2018) 69–77.
[20] R.K. Jian, Y.F. Ai, L. Xia, L.J. Zhao, H.B. Zhao, Single component phosphamide-based intumescent flame retardant with potential reactivity towards low flammability and smoke epoxy resins, J. Hazard Mater. 371 (2019) 529–539.
[21] L.S. Zhou, G.C. Zhang, Y.J. Feng, H.M. Zhang, J.T. Li, X.T. Shi, Design of a self-healing and flame-retardant cyclotriphosphazene-based epoxy vitrimer, J. Mater. Sci. 53 (9) (2018) 7030–7047.
[22] L. Gu, G. Chen, Y. Yao, Two novel phosphorus–nitrogen-containing halogen-free flame retardants of high performance for epoxy resin, Polym. Degrad. Stab. 108 (2014) 68–75.
[23] C.H. Lin, H.T. Lin, J.W. Sie, K.Y. Hwang, A.P. Tu, Facile, one-pot synthesis of aromatic diamine-based phosphinated benzoxazines and their flame-retardant thermosets, J. Polym. Sci., Polym. Chem. Ed. 48 (20) (2010) 4555–4566.
[24] V. Bellenger, E. Fontaine, A. Fleishmann, J. Saporito, J. Verdu, Thermogravimetric study of amine cross-linked epoxies, Polym. Degrad. Stab. 9 (4) (1984) 195–208.
[25] M. Wang, S. Fang, H. Zhang, Study on flame retardancy of TGDDM epoxy resin blended with inherent flame-retardant epoxy ether, High Perform. Polym. 30 (3) (2017) 318–327.
[26] X. Wang, S. Zhou, W.W. Guo, P.L. Wang, W.Y. Xing, L. Song, et al., Renewable cardanol-based phosphate as a flame retardant toughening agent for epoxy resins, ACS Sustain. Chem. Eng. 5 (4) (2017) 3409–3416.
[27] W.H. Xu, A. Wirasaputra, S.M. Liu, Y.C. Yuan, J.Q. Zhao, Highly effective flame retarded epoxy resin cured by DOPO-based co-curing agent, Polym. Degrad. Stab. 122 (2015) 44–51.
[28] P. Wang, F.S. Yang, L. Li, Z.S. Cai, Flame-retardant properties and mechanisms of epoxy thermosets modified with two phosphorus-containing phenolic amines, J. Appl. Polym. Sci. 133 (37) (2016) 43953–43966.
[29] S.Q. Huo, Z.T. Liu, C. Li, X.L. Wang, H.P. Cai, J. Wang, Synthesis of a phosphaphenanthrene/benzimidazole-based curing agent and its application in flame-retardant epoxy resin, Polym. Degrad. Stab. 163 (2019) 100–109.
[30] J.L. Li, H.Y. Wang, S.C. Li, A novel phosphorus–silicon containing epoxy resin with enhanced thermal stability, flame retardancy and mechanical properties, Polym. Degrad. Stab. 164 (2019) 36–45.
[31] S. Nagendiran, M. Alagar, I. Hamerton, Octasilsesquioxane-reinforced DGEBA and TGDDM epoxy nanocomposites: characterization of thermal, dielectric and morphological properties, Acta Mater. 58 (9) (2010) 3345–3356.
[32] H.J. Duan, Y.S. Chen, S. Ji, R. Hu, H.R. Ma, A novel phosphorus/nitrogen-containing polycarboxylic acid endowing epoxy resin with excellent flame retardance and mechanical properties, Chem. Eng. J. 375 (2019) 121916–121927.
[33] Y. Wen, Z. Cheng, W.X. Li, Z. Li, D.J. Liao, X.P. Hu, et al., A novel oligomer containing DOPO and ferrocene groups: synthesis, characterization, and its application in fire retardant epoxy resin, Polym. Degrad. Stab. 156 (2018) 111–124.
[34] G. Yang, W.H. Wu, Y.H. Wang, Y.H. Jiao, L.Y. Lu, H.Q. Qu, et al., Synthesis of a novel phosphazene-based flame retardant with active amine groups and its application in reducing the fire hazard of Epoxy Resin, J. Hazard Mater. 366 (2019) 78–87.
[35] S.L. Qiu, Y.F. Zhou, X. Zhou, T. Zhang, C.Y. Wang, R.K.K. Yuen, et al., Air-stable polyphosphazene-functionalized few-layer black phosphorene for flame retardancy of epoxy resins, Small 15 (10) (2019) 1805175–1805187.
[36] W.G. Liu, S.Q. Wang, S. Dasgupta, S.T. Thynell, W.A. Goddard, S. Zybin, et al., Experimental and quantum mechanics investigations of early reactions of monomethylhydrazine with mixtures of NO_2 and N_2O_4, Combust. Flame 160 (5) (2013) 970–981.
[37] L.C. Speitel, Fourier transform infrared analysis of combustion gases, J. Fire Sci. 20 (5) (2002) 349–371.
[38] R.K. Jian, P. Wang, L. Xia, X.Q. Yu, X.L. Zheng, Z.B. Shao, Low-flammability epoxy resins with improved mechanical properties using a Lewis base based

on phosphaphenanthrene and 2-aminothiazole, J. Mater. Sci. 52 (16) (2017) 9907–9921.
[39] S.N. Li, X.J. Zhao, X.H. Liu, X. Yang, R. Yu, Y. Zhang, et al., Cage–ladder-structure, phosphorus-containing polyhedral oligomeric silsesquinoxanes as promising reactive-type flame retardants for epoxy resin, J. Appl. Polym. Sci. 136 (23) (2019) 47607.
[40] Y. Qiu, L.J. Qian, W. Xi, Flame-retardant effect of a novel phosphaphenanthrene/triazine-trione bi-group compound on an epoxy thermoset and its pyrolysis behaviour, RSC Adv. 6 (61) (2016) 56018–56027.
[41] A.I. Balabanovich, D. Pospiech, L. Häußler, C. Harnisch, M. Döring, Pyrolysis behavior of phosphorus polyesters, J. Anal. Appl. Pyrolysis 86 (1) (2009) 99–107.
[42] A. Gooneie, P. Simonetti, K.A. Salmeia, S. Gaan, R. Hufenus, M.P. Heuberger, Enhanced PET processing with organophosphorus additive: flame retardant products with added-value for recycling, Polym. Degrad. Stab. 160 (2019) 218–228.
[43] Y. Qiu, L.J. Qian, H.S. Feng, S.L. Jin, J.W. Hao, Toughening effect and flame-retardant behaviors of phosphaphenanthrene/phenylsiloxane bigroup macromolecules in epoxy thermoset, Macromolecules 51 (23) (2018) 9992–10002.
[44] X.X. Tao, H.J. Duan, W.J. Dong, X. Wang, S. Yang, Synthesis of an acrylate constructed by phosphaphenanthrene and triazine-trione and its application in intrinsic flame retardant vinyl ester resin, Polym. Degrad. Stab. 154 (2018) 285–294.
[45] S. Tang, L.J. Qian, Y. Qiu, Y.P. Dong, High-performance flame retardant epoxy resin based on a bi-group molecule containing phosphaphenanthrene and borate groups, Polym. Degrad. Stab. 153 (2018) 210–219.
[46] W.J. Liang, B. Zhao, P.H. Zhao, C.Y. Zhang, Y.Q. Liu, Bisphenol-S bridged penta(anilino)cyclotriphosphazene and its application in epoxy resins: synthesis, thermal degradation, and flame retardancy, Polym. Degrad. Stab. 135 (2017) 140–151.
[47] B. Schartel, B. Perret, B. Dittrich, M. Ciesielski, J. Krämer, P. Müller, et al., Flame retardancy of polymers: the role of specific reactions in the condensed phase, Macromol. Mater. Eng. 301 (1) (2016) 9–35.
[48] J.J. Zhao, X. Dong, S. Huang, X.J. Tian, L. Song, Q. Yu, et al., Performance comparison of flame retardant epoxy resins modified by DPO–PHE and DOPO–PHE, Polym. Degrad. Stab. 156 (2018) 89–99.
[49] E. Gallo, B. Schartel, U. Braun, P. Russo, D. Acierno, Fire retardant synergisms between nanometric Fe_2O_3 and aluminum phosphinate in poly(butylene terephthalate), Polym. Adv. Technol. 22 (12) (2011) 2382–2391.
[50] S.B. Yang, L.J. Zhi, K. Tang, X.L. Feng, J. Maier, K. Müllen, Efficient synthesis of heteroatom (N or S)-Doped graphene based on ultrathin graphene oxide-porous silica sheets for oxygen reduction reactions, Adv. Funct. Mater. 22 (17) (2012) 3634–3640.
[51] R.X. Chu, J. Lin, C.Q. Wu, J. Zheng, Y.L. Chen, J. Zhang, et al., Reduced graphene oxide coated porous carbon–sulfur nanofiber as a flexible paper electrode for lithium–sulfur batteries, Nanoscale 9 (26) (2017) 9129–9138.
[52] Y.Y. Gao, C. Deng, Y.Y. Du, S.C. Huang, Y.Z. Wang, A novel bio-based flame retardant for polypropylene from phytic acid, Polym. Degrad. Stab. 161 (2019) 298–308.
[53] Z.N. Li, M.F. Chen, S.S. Li, X.M. Fan, C.P. Liu, Simultaneously improving the thermal, flame-retardant and mechanical properties of epoxy resins modified by a novel multi-element synergistic flame retardant, Macromol. Mater. Eng. 304 (4) (2019) 1800619–1800628.